

Electric field modification of magnetotransport in Ni thin films on (011) PMN-PT piezosubstrates

Cite as: Appl. Phys. Lett. **106**, 062404 (2015); <https://doi.org/10.1063/1.4907775>

Submitted: 22 December 2014 . Accepted: 28 January 2015 . Published Online: 10 February 2015

Alexander Tkach, Andreas Kehlberger, Felix Büttner, Gerhard Jakob, Stefan Eisebitt, and Mathias Kläui



View Online



Export Citation



CrossMark

ARTICLES YOU MAY BE INTERESTED IN

Domain engineered switchable strain states in ferroelectric (011) $[\text{Pb}(\text{Mg}_{1/3}\text{Nb}_{2/3})\text{O}_3]_{(1-x)}-[\text{PbTiO}_3]_x$ (PMN-PT, $x \approx 0.32$) single crystals

Journal of Applied Physics **109**, 124101 (2011); <https://doi.org/10.1063/1.3595670>

Giant electric-field-induced reversible and permanent magnetization reorientation on magnetoelectric Ni/(011) $[\text{Pb}(\text{Mg}_{1/3}\text{Nb}_{2/3})\text{O}_3]_{(1-x)}-[\text{PbTiO}_3]_x$ heterostructure

Applied Physics Letters **98**, 012504 (2011); <https://doi.org/10.1063/1.3534788>

Electrical switching of the magnetic vortex circulation in artificial multiferroic structure of Co/Cu/PMN-PT(011)

Applied Physics Letters **110**, 262405 (2017); <https://doi.org/10.1063/1.4990987>

Lock-in Amplifiers
up to 600 MHz



Electric field modification of magnetotransport in Ni thin films on (011) PMN-PT piezosubstrates

Alexander Tkach,^{1,2} Andreas Kehlberger,^{1,3} Felix Büttner,^{1,3,4} Gerhard Jakob,^{1,3} Stefan Eisebitt,⁴ and Mathias Kläui^{1,3}

¹*Institute of Physics, Johannes Gutenberg University, Staudinger Weg 7, 55128 Mainz, Germany*

²*CICECO – Aveiro Institute of Materials, Department of Materials and Ceramic Engineering, University of Aveiro, 3810-093 Aveiro, Portugal*

³*Graduate School of Excellence Materials Science in Mainz, Staudinger Weg 9, 55128 Mainz, Germany*

⁴*Institute of Optics and Atomic Physics, Technical University of Berlin, Str. des 17 Juni 135, 10623 Berlin, Germany*

(Received 22 December 2014; accepted 28 January 2015; published online 10 February 2015)

This study reports the magnetotransport and magnetic properties of 20 nm-thick polycrystalline Ni films deposited by magnetron sputtering on unpoled piezoelectric (011) $[\text{PbMg}_{1/3}\text{Nb}_{2/3}\text{O}_3]_{0.68}\text{--}[\text{PbTiO}_3]_{0.32}$ (PMN-PT) substrates. The longitudinal magnetoresistance (MR) of the Ni films on (011) PMN-PT, measured at room temperature in the magnetic field range of $-0.3\text{ T} < \mu_0 H < 0.3\text{ T}$, is found to depend on the crystallographic direction and polarization state of piezosubstrate. Upon poling the PMN-PT substrate, which results in a transfer of strain to the Ni film, the MR value decreases by factor of 20 for the current along $[100]$ of PMN-PT and slightly increases for the $[01\bar{1}]$ current direction. Simultaneously, a strong increase (decrease) in the field value, where the MR saturates, is observed for the $[01\bar{1}]$ ($[100]$) current direction. The anisotropic magnetoresistance is also strongly affected by the remanent strain induced by the electric field pulses applied to the PMN-PT in the non-linear regime revealing a large (132 mT) magnetic anisotropy field. Applying a critical electric field of 2.4 kV/cm, the anisotropy field value changes back to the original value, opening a path to voltage-tuned magnetic field sensor or storage devices. This strain mediated voltage control of the MR and its dependence on the crystallographic direction is correlated with the results of magnetization reversal measurements. © 2015 AIP Publishing LLC.

[<http://dx.doi.org/10.1063/1.4907775>]

The conventional control of magnetization by current-generated magnetic fields is disadvantageous for electronic devices and sensors due to difficulties in reducing power consumption and realizing device miniaturization resulting from poor scaling. The non-volatile voltage control of the magnetization, resistivity or magnetoresistance (MR) in multiferroic heterostructures is one of the most promising schemes for achieving energy-efficient electronic applications.¹ Such artificial multiferroics consist of ferro(i)magnetic and ferroelectric layers and parameters of the former one are controlled by a polarization of the latter one switched by external electric field with maximum energy efficiency.² There are numerous reports on voltage control of magnetization (see, e.g., reviews,^{1–4} references therein, and recent Refs. 5–11), whereas for electric field effects on the anisotropic^{12–20} and giant^{13,21,22} MR in magnetic/ferroelectric heterostructures only few reports exist.

Recently, much attention has been focused on strain-mediated magnetoelectric coupling between high- T_c ferro(i)magnetic films such as Ni, Ni-Fe, or Fe_3O_4 and (011)-oriented ferroelectric substrates with high room-temperature piezoelectric coefficients such as $[\text{PbMg}_{1/3}\text{Nb}_{2/3}\text{O}_3]_{1-x}\text{--}[\text{PbTiO}_3]_x$ (PMN-PT) or $[\text{PbZn}_{1/3}\text{Nb}_{2/3}\text{O}_3]_{1-x}\text{--}[\text{PbTiO}_3]_x$ (PZN-PT).^{4–11,13,14,16,17,20} In such structures, upon application of an electric field, the piezoactive substrate induces a strain in the ferro(i)magnetic film and hence modifies its magnetic properties due to the magnetoelastic coupling effect. The (011) cut is particularly suitable because of the possibility of obtaining a

high and well-defined uniaxial anisotropy by inducing simultaneously compressive and tensile strains in orthogonal $[100]$ (x) and $[01\bar{1}]$ (y) in-plane directions due to the different signs of d_{31} and d_{32} piezocoefficients.^{5,13} Voltage control of magnetization has been widely studied for Ni films on (011) PMN-PT using magneto-optic Kerr effect (MOKE) magnetometry and magnetic imaging,^{7–9,11} whereas the electric field effects on the MR have only been studied in detail for magnetite^{16,20} and permalloy films¹⁷ on (011) PMN-PT. Additionally, the MR response of permalloy films as a function of the electric field applied to the (011) PZN-PT piezosubstrate has been reported.^{13,14} Permalloy exhibits, however, a small magnetoelastic coupling constant, while its study on PMN-PT was made available only at finite magnetic fields.¹⁷ Moreover, to be useful for a device, one needs a change of the resistance at zero applied voltage, which has not been demonstrated using the application-relevant electrical readout. Furthermore, for 3d-metals, Ni exhibits the highest magnetoelastic coupling and is thus the material of choice where, by determining the full field dependence of the magnetotransport properties, one can gauge the applicability of this approach.

In this work, we report the results of magnetotransport characterization of 20 nm-thick polycrystalline Ni films deposited by magnetron sputtering on unpoled (011)-oriented PMN-PT piezosubstrates. We determine the variation of the magnetotransport with the induced changes in the magnetic anisotropy resulting from the strain generated by PMN-PT poling and reversible and irreversible non-volatile switching

by electric fields, and correlate the magnetoresistance changes with the magnetization manipulation.

The samples were prepared on polished (011)-oriented $[\text{PbMg}_{1/3}\text{Nb}_{2/3}\text{O}_3]_{1-x}[\text{PbTiO}_3]_x$ ($x = 0.32$) substrates (Atom Optics Co., Ltd., Shanghai, China) of $5 \times 5 \times 0.5 \text{ mm}^3$ size that were annealed at 300°C for 30 min. First, top (10 nm) and bottom (50 nm) Pt layers were DC-magnetron sputtered on both sides of the PMN-PT substrate using 5 nm-thick adhesion layers of Cr. Then, polycrystalline Ni films with a thickness of 20 nm were deposited on the top side by DC-magnetron sputtering using an Ar pressure of 10^{-2} mbar.

Magnetoresistance measurements were performed in a van der Pauw configuration within a He cryostat (Oxford Instruments, MicrostatHe), using a system electrometer (Keithley 6514) as a current source and a 6.5-digit multimeter (Agilent 34411A) as a voltmeter with an error for our measurement range of $\sim 0.02\%$. The magnetic field up to 0.3 T was generated by an electromagnet (GMW 3470) powered by a bipolar power supply (Kepco BOP 36–6M). A voltage supply (FuG) was used for application of the electric fields up to 4 kV/cm between the top (Ni film) and bottom (Pt) electrodes of PMN-PT. The magnetization loops were obtained by a superconducting quantum interference device (SQUID) magnetometer (Quantum Design MPMSXL) along the x [100] and y [01 $\bar{1}$] directions with further subtraction of substrate diamagnetic component.

Figure 1 shows the room-temperature longitudinal magnetoresistance ratio $\Delta R/R_0 = [R(H) - R_0]/R_0$ (R_0 denotes the resistivity at the coercive field, i.e., for a vanishing net magnetization) of the Ni film on (011) PMN-PT as a function of the magnetic field H applied together with the current J along the y (Figs. 1(a) and 1(b)) and x (Fig. 1(c)) sample axes under several electric fields applied to PMN-PT. Increasing the electric field from 0 to 1.6 kV/cm, a slight increase of the saturation MR (MR_{max}) value from 1.68% to 1.81% is detected, as shown in Fig. 1(a). Further application of the 2.4 kV/cm field leads to the poling of PMN-PT, accompanied by its abrupt deformation and hence by a strong strain-induced modification of the MR response of Ni film. A much higher MR_{max} value of 2.34% and the significantly larger magnetic field, at which the MR saturates, (H_s) are visible. An increase of the electric field to 4 kV/cm yields no further considerable change in the MR_{max} but an increase in H_s , while subsequent decrease of the electric field down to 0 kV/cm leads to a decrease of H_s . Moreover, the H_s value continues to decrease on subsequent application of negative voltage of -2.4 kV/cm, as shown in Fig. 1(b). This variation of the applied electric field is accompanied by a decrease of the MR_{max} value from 2.27% to 1.96%, implying an approximation to the coercive electric field, at which PMN-PT is near to the zero-polarization state and hence the Ni film on top of PMN-PT is under the unstrained condition, again showing approximate reversibility. However, applying then -4 kV/cm, we pole the piezoelectric substrate in opposite out-of-plane direction and obtain again the high MR_{max} value of 2.2% and the large H_s , as expected from the symmetry of the poling.

Figure 1(c) shows the longitudinal MR of Ni film along the x direction under the same electric fields applied to PMN-PT (previously poled by 4 kV/cm) as presented in

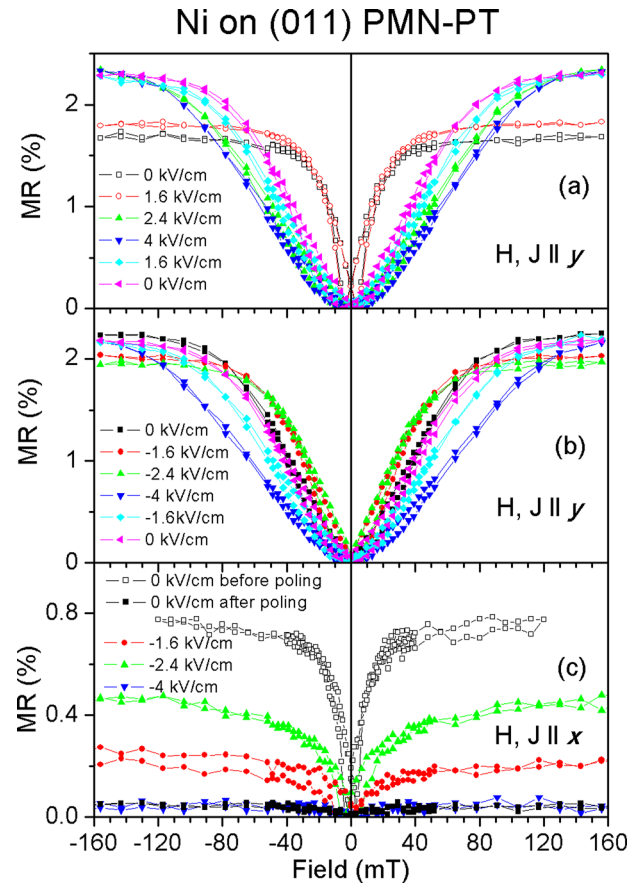


FIG. 1. Room-temperature magnetoresistance ratio $\Delta R/R_0$ of the Ni film on (011) PMN-PT as a function of magnetic field applied together with current along the y ((a) and (b)) and x (c) in-plane directions, measured under positive electric fields varying as 0, 1.6, 2.4, 4, 1.6, and 0 kV/cm (a) and under negative electric fields varying as 0, -1.6 , -2.4 , -4 , -1.6 , and 0 kV/cm (b). In (c), we show the sequence for 0 (before poling), 0 (after poling with 4 kV/cm), and then -1.6 , -2.4 , -4 kV/cm, applied to the piezoelectric substrate. The lines connecting points are guides to the eye.

Fig. 1(b) for the y direction. For comparison, the MR response of the unpoled sample is depicted as well. We show that we can nearly completely suppress the MR response, poling PMN-PT, as the change in the MR response along x is reduced by a factor of ~ 20 from 0.78% to 0.04%. Upon further application of -1.6 kV/cm and -2.4 kV/cm, the MR_{max} value changes towards the unpoled one, reaching 0.22% and 0.46%, respectively. However, subsequently applying -4 kV/cm, we suppress the MR_{max} again showing that this effect is again reproducible and reversible. A factor of 4 suppression of the MR ratio and a decrease of the saturation field by application of the 4 kV/cm electric field were observed as well for $\text{Ni}_{80}\text{Fe}_{20}/\text{PZN-PT}$ heterostructures.¹⁴

In Figure 2, we analyze the variation of the MR_{max} and H_s values with the electric field. Results presented by solid symbols reveal a clear poling step around 2.4 kV/cm and a “butterfly” like loop with the coercive electric field of -2.4 kV/cm. Such a critical field value was also observed in the electric field dependence of the strain induced in the PMN-PT crystals of the same type and manufacturer.⁹ Moreover, the approximately linear variation of the H_s with electric field decreasing from 4 kV/cm to 0 is in a qualitative agreement with the variation of the anisotropy field of Ni films on PMN-PT as a function of the electric field, deduced

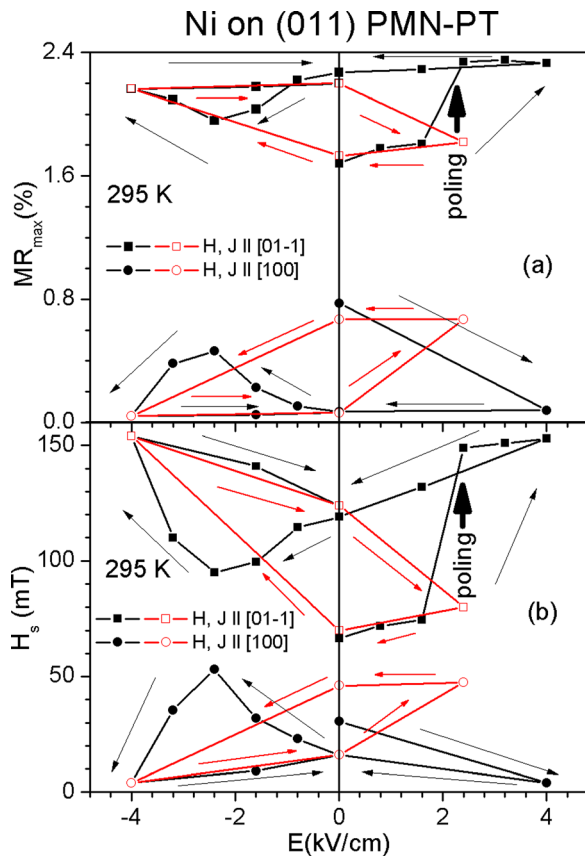


FIG. 2. Saturation longitudinal magnetoresistance value MR_{\max} (a) and field H_s (b) of the Ni film on (011) PMN-PT with magnetic field and current along the y (squares) and x (circles) in-plane directions as a function of electric fields applied to the piezsubstrate in $0 \rightarrow 4 \rightarrow -4 \rightarrow 0$ kV/cm sequence (solid symbols) and in $-4 \rightarrow 0 \rightarrow 2.4 \rightarrow 0$ kV/cm sequence (open symbols). The lines connecting points are guides to the eye.

from MOKE magnetometry.⁶ Furthermore, a monotonous variation of H_s with electric field was also observed for the MR response of $Ni_{80}Co_{20}/PZN$ -PT heterostructure.¹³ However, here we show by electrical read-out that we can change the magnetoresistance irreversibly and obtain different magnetoresistance values in a non-volatile manner at zero applied electric field, which has not been reported so far but is important for practical applications. Thus, knowing the value of the critical electric field, we have measured the MR of the Ni film on (011) PMN-PT at zero electric field after application of -4 kV/cm (maximum residual strain in the poled state) and subsequent application of 2.4 kV/cm (minimum residual strain in the close to zero polarization state) to the piezsubstrate. As shown in Figure 3(a), the measurements were performed in both y and x current directions and both longitudinal and transverse geometries and compared to the results obtained in the unpoled state. Both directions are found to exhibit a typical anisotropic MR (AMR) curve. The resistivity of the Ni film in the longitudinal (transverse) direction shows minima (maxima) near the coercive field of ~ 4 mT, increases (decreases), and saturates to a constant value MR_{\max} above the saturation field H_s . However, the parameters of the MR response (MR_{\max} and H_s) depend sensitively on the magnetic field direction. When the magnetic field is along y , the absolute values of MR_{\max} and H_s are higher than that for magnetic field along x . Moreover, these

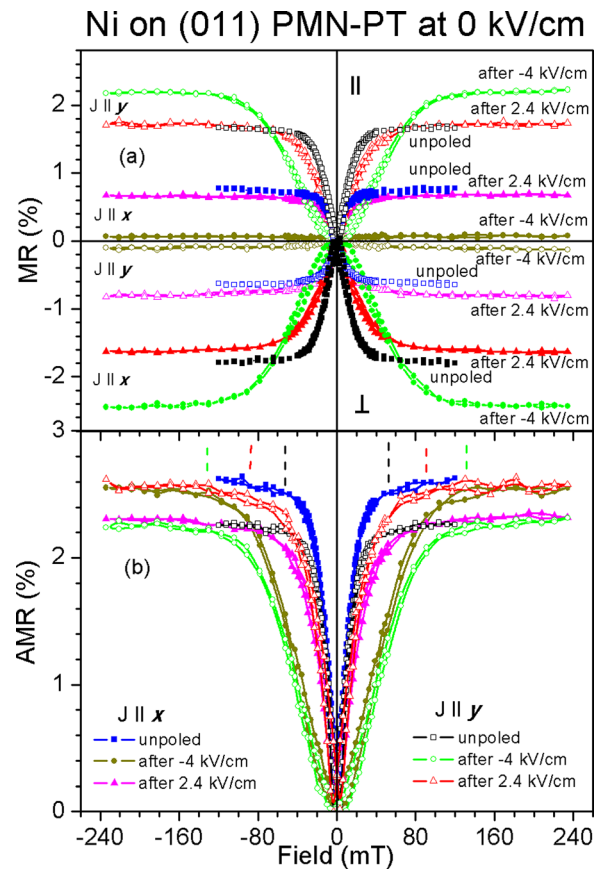


FIG. 3. Room-temperature magnetoresistance ratio $\Delta R/R_0$ in longitudinal (||) and transverse (⊥) geometries (a) and anisotropic magnetoresistance (b) of the Ni film on (011) PMN-PT in unpoled state (squares), after poling with application of the -4 kV/cm electric field (circles), and after subsequent application of the 2.4 kV/cm electric field (triangles) as function of magnetic field, measured with the current along the x (solid symbols) and y (open symbols) in-plane directions. Dashed lines mark the anisotropy fields. The lines connecting points are guides to the eye.

values increase after the application of the -4 kV/cm electric field and decrease close to the initial value in the unpoled state after further application of the 2.4 kV/cm electric field for both y and x currents. In contrast, MR_{\max} diminishes upon poling and recovers at de-poling for the magnetic field aligned along x . Such asymmetric hysteretic behavior of the MR parameters as a function of electric field is presented by the open symbols in Figure 2 for the longitudinal MR.

Using the results plotted in Figure 3(a), the anisotropic magnetoresistance was defined as $AMR = [R_{\text{long}} - R_{\text{trans}}] / [R_{\text{long}}/3 + 2 \cdot R_{\text{trans}}/3]$, where R_{long} and R_{trans} are the resistances for magnetic field applied parallel and perpendicular to the current direction, respectively. Figure 3(b) shows the room-temperature AMR ratio of the Ni film on (011) PMN-PT in unpoled state, after poling by the application of -4 kV/cm and after subsequent application of 2.4 kV/cm for the currents along x and y . For all the cases, the maximum AMR values are similar, varying between 2.31% and 2.62% , and being just slightly smaller than $\sim 3\%$ observed for a $Ni_{77}Fe_{23}/PMN$ -PT heterostructure.¹⁷ The effect of the electric field pulse application is mainly reflected in the modification of the anisotropy field H_a (marked in Fig. 3(b) by dashed lines) when the magnetization is aligned with the applied magnetic field. Upon poling, H_a value increases from

~ 54 mT to ~ 132 mT as observed for both x and y current directions. Further application of the 2.4 kV/cm pulse leads to the decrease of H_a to ~ 87 mT.

To understand the results, we compare the observed field-dependence with magnetometry. We find that the variation of H_a is confirmed by the magnetization loop measurements of Ni films on PMN-PT as presented in Figure 4. In the unpoled state (Fig. 4(a)), the magnetization loop for the x magnetic field direction is just slightly smaller than that for the y direction and both loops merge at magnetic field as low as ~ 60 mT that is near the H_a value deduced from the transport measurements. After application of the -4 kV/cm electric field (Fig. 4(b)), the loops become distinctly different. In the y magnetic field direction, it is more square-shaped, while along x the loop is slanted. So the loops merge at much larger H_a value close to 130 mT, in agreement with the AMR analysis. Finally, further application of a 2.4 kV/cm electric field (Fig. 4(c)) leads to a partial recovery of the initial magnetic state with H_a of ~ 90 mT. This means that we have achieved a non-volatile permanent magnetization change that is reflected in the magnetotransport properties.

At the same time, the coercive magnetic field (H_c) values, which are deduced from the magnified loops as shown in Figure 5, reveal a good correlation with the H_s parameter of the longitudinal MR, presented in Figure 2(b). After poling, H_c increases from 4.1 mT to 8.8 mT (H_s increases from 66.5 mT to 124 mT) along y and slightly

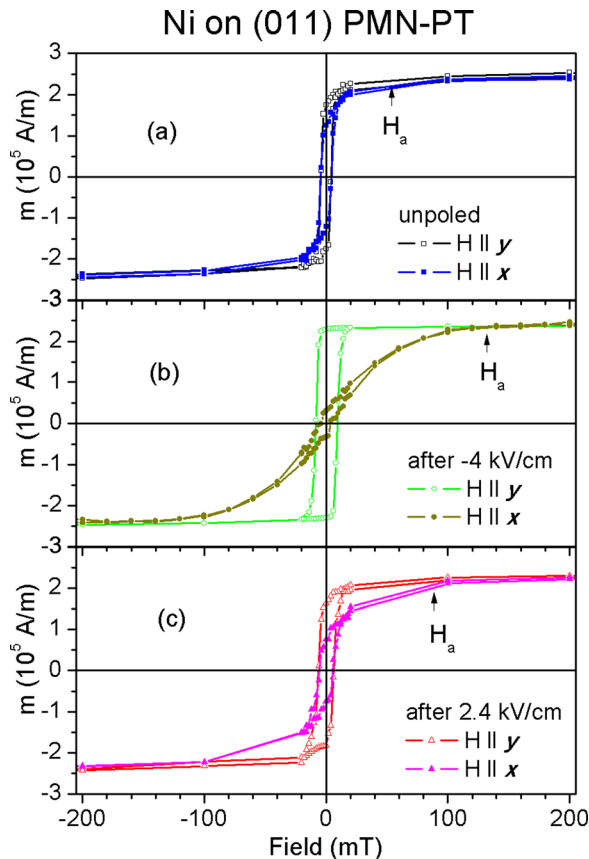


FIG. 4. Room-temperature magnetization loops of the Ni film on (011) PMN-PT, measured by the SQUID along the x (solid symbols) and y (open symbols) directions in unpoled state (a), after poling with application of the -4 kV/cm electric field (b), and after subsequent application of the 2.4 kV/cm electric field (c). The lines connecting points are guides to the eye.

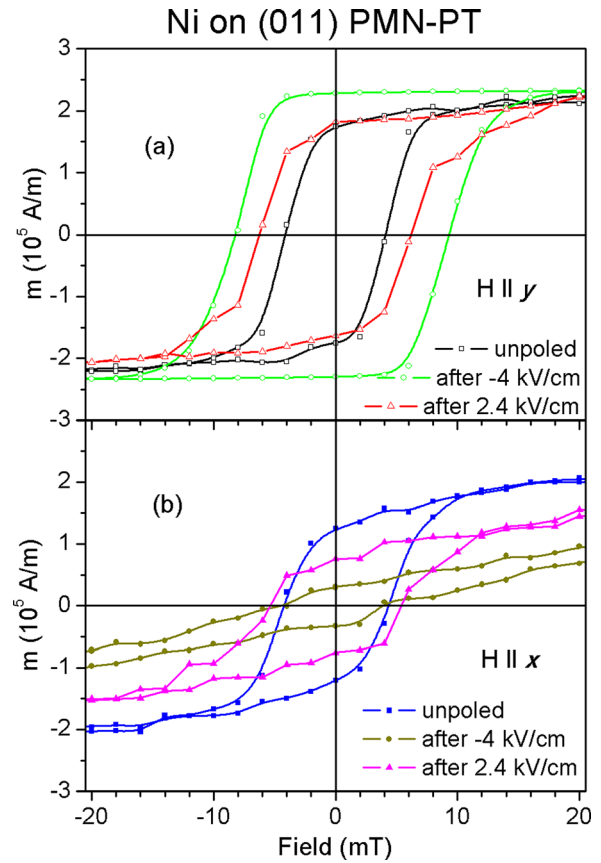


FIG. 5. Magnified room-temperature magnetization loops of the Ni film on (011) PMN-PT, measured by the SQUID along the y (a, open symbols) and x (b, solid symbols) directions unpoled state (squares), after poling with application of the -4 kV/cm electric field (circles), and after subsequent application of the 2.4 kV/cm electric field (triangles). The lines connecting points are guides to the eye.

decreases from 4.3 mT to 4.2 mT (H_s decreases from 30.5 mT to 16 mT) along x . After the application of 2.4 kV/cm subsequent to -4 kV/cm, H_c decreases to 6.2 mT (H_s decreases to 70 mT) in the y direction and increases to 5.4 mT (H_s decreases to 46 mT) in the x direction. In agreement with our results, a coercivity of ~ 3.5 mT was reported for the as-deposited Ni film on LiNbO_3 substrate along the y direction, while the electric poling induced the remanent strain change, yielding an H_c of ~ 8 mT.⁶

Instead of the previously used semi-quantitative MOKE magnetometry,^{7,8} here we use a fully quantitative SQUID technique to determine not only the critical magnetic field values but also a saturation magnetization and anisotropy constants quantitatively. Thus, determining the saturation magnetization value as 255 ± 15 kA/m and taking the H_a values deduced from MR study, the absolute value of an anisotropy constant, estimated as their product divided by 2,^{23,24} is found to be ~ 7 kJ/m³ for unpoled state, ~ 17 kJ/m³ after poling, and ~ 11 kJ/m³ after de-poling pulse. Such variation of the anisotropy constant is in good agreement with the magnetoelastic anisotropy up to 16 kJ/m³ induced by poling the (011) PMN-PT.⁹

In conclusion, we have demonstrated a very large effect of the poling of (011) PMN-PT piezosubstrates on the magnetic anisotropy and magnetotransport properties of Ni films at room temperature. The anisotropy field and thus

anisotropy constant are increased ~ 2.5 times. At the same time, the longitudinal magnetoresistance is reduced by a factor of ~ 20 for the x current direction, indicating an induced hard axis, and increased for the y current direction, indicating an easy axis. The modification of the MR response by the applied electric field was attributed to a change in the strain-induced anisotropy of the films induced by the PMN-PT substrate with piezocoefficients of different signs in orthogonal in-plane x and y directions. Moreover, we have shown a reversible and non-volatile variation of the magnetic anisotropy in the Ni films on (011) PMN-PT using voltage pulses in the non-linear regime of the piezoelectric PMN-PT. This allows us to switch the magnetotransport and magnetic behavior of the Ni films between the poled high strain state and near-zero-polarization low strain state. The magnetic anisotropy induced by poling and switching of the magnetotransport and magnetic properties provides a promising approach for magnetic field sensor and memory applications.

This work was funded by the EU's 7th Framework Program IFOX (NMP3-LA-2010 246102), the Graduate School of Excellence MAINZ (GSC 266 Mainz), the German Science Foundation (DFG), and the ERC (2007-Stg 208162). A. Tkach also acknowledges funds by FEDER through Programa Operacional Factores de Competitividade—COMPETE, and national funds through FCT—Fundação para a Ciência e Tecnologia within CICECO project—FCOMP-01-0124-FEDER-037271 (FCT Ref. PEst-C/CTM/LA0011/2013) and independent researcher Grant No. IF/00602/2013.

¹J. Ma, J. Hu, Z. Li, and C.-W. Na, *Adv. Mater.* **23**, 1062 (2011).

²C. A. F. Vaz, *J. Phys.: Condens. Matter* **24**, 333201 (2012).

³J. T. Heron, D. G. Schlom, and R. Ramesh, *Appl. Phys. Rev.* **1**, 021303 (2014).

⁴M. Liu and N. X. Sun, *Philos. Trans. R. Soc., A* **372**, 20120439 (2014).

⁵M. Liu, O. Obi, J. Lou, Y. Chen, Z. Cai, S. Stoute, M. Espanol, M. Lew, X. Situ, K. S. Ziemer, V. G. Harris, and N. X. Sun, *Adv. Funct. Mater.* **19**, 1826 (2009).

⁶T. Wu, A. Bur, J. L. Hockel, K. Wong, T.-K. Chung, and G. P. Carman, *IEEE Magn. Lett.* **2**, 6000104 (2011).

⁷T. Wu, A. Bur, K. Wong, J. L. Hockel, C.-J. Hsu, H. K. D. Kim, K. L. Wang, and G. P. Carman, *J. Appl. Phys.* **109**, 07D732 (2011).

⁸T. Wu, A. Bur, P. Zhao, K. P. Mohanchandra, K. Wong, K. L. Wang, C. S. Lynch, and G. P. Carman, *Appl. Phys. Lett.* **98**, 012504 (2011).

⁹J. L. Hockel, A. Bur, T. Wu, K. P. Wetzlar, and G. P. Carman, *Appl. Phys. Lett.* **100**, 022401 (2012).

¹⁰H. K. D. Kim, L. T. Schelhas, S. Keller, J. L. Hockel, S. H. Tolbert, and G. P. Carman, *Nano Lett.* **13**, 884 (2013).

¹¹S. Finizio, M. Foerster, M. Buzzi, B. Krüger, M. Jourdan, C. A. F. Vaz, J. Hockel, T. Miyawaki, A. Tkach, S. Valencia, F. Kronast, G. P. Carman, F. Nolting, and M. Kläui, *Phys. Rev. Appl.* **1**, 021001 (2014).

¹²V. Laukhin, V. Skumryev, X. Marti, D. Hrabovsky, F. Sanchez, M. V. Garcia-Cuenca, C. Ferrater, M. Varela, U. Luders, J. F. Bobo, and J. Fontcuberta, *Phys. Rev. Lett.* **97**, 227201 (2006).

¹³M. Liu, S. Li, O. Obi, J. Lou, S. Rand, and N. X. Sun, *Appl. Phys. Lett.* **98**, 222509 (2011).

¹⁴M. Liu, O. Obi, J. Lou, S. Li, X. Xing, G. Yang, and N. X. Sun, *J. Appl. Phys.* **109**, 07D913 (2011).

¹⁵A. Brandlmaier, S. Geprags, G. Woltersdorf, R. Gross, and S. T. B. Goennenwein, *J. Appl. Phys.* **110**, 043913 (2011).

¹⁶M. Liu, J. Hoffman, J. Wang, J. Zhang, B. Nelson-Cheeseman, and A. Bhattacharya, *Sci. Rep.* **3**, 1876 (2013).

¹⁷Y. Gao, J. Hu, L. Shu, and C. W. Nan, *Appl. Phys. Lett.* **104**, 142908 (2014).

¹⁸D. Preziosi, I. Fina, E. Pippel, D. Hesse, X. Marti, F. Bern, M. Ziese, and M. Alexe, *Phys. Rev. B* **90**, 125155 (2014).

¹⁹J. H. Lee, I. Fina, X. Marti, Y. H. Kim, D. Hesse, and M. Alexe, *Adv. Mater.* **26**, 7078 (2014).

²⁰A. Tkach, M. Baghaie Yazdi, M. Foerster, F. Büttner, M. Vafaei, M. Fries, and M. Kläui, *Phys. Rev. B* **91**, 024405 (2015).

²¹J. Allibe, S. Fusil, K. Bouzehouane, C. Daumont, D. Sando, E. Jacquet, C. Deranlot, M. Bibes, and A. Barthélemy, *Nano Lett.* **12**, 1141 (2012).

²²H. Kojima, T. Naito, H. Muraoka, E. Wada, I. Suzuki, Y. Shirahata, M. Itoh, and T. Taniyama, *J. Appl. Phys.* **113**, 17C713 (2013).

²³E. C. Stoner and E. P. Wohlfarth, *Philos. Trans. R. Soc., A* **240**, 599 (1948).

²⁴M. Ziese, I. Vrejoiu, and D. Hesse, *Phys. Rev. B* **81**, 184418 (2010).